INTEGRAL

Announcement of Opportunity for Observing Proposals (AO-3)

IBIS Observer's Manual

Written by: E. Kuulkers

Integral Science Operations, ESTEC

Based upon inputs from:
P. Ubertini, IBIS Co-P.I., IAS-CNR, Rome
F. Lebrun, IBIS Co-P.I., CEA, Saclay
A. Bazzano, IAS-CNR, Rome
L. Natalucci, IAS-CNR, Rome
J. Lockley, University of Southampton
P. Barr, Integral Science Operations, ESTEC

13 September 2004

Issue 3

This page was intentionally left blank

Table of Contents

I. Introduction

IBIS (**I**mager on **B**oard the **I**NTEGRAL **S**atellite) is one of the two prime instruments of the INTEGRAL scientific payload.

IBIS is a gamma-ray telescope which is able to observe celestial objects of all classes ranging from the most compact galactic systems to extra-galactic objects, with powerful diagnostic capabilities of fine imaging, source identification and spectral sensitivity in both continuum and lines. It covers the entire energy range from about 15 keV to several MeV, and it can localise weak sources at low energies to better than a few arcminutes accuracy.

Table 1 gives an overview of the scientific capabilities of IBIS.

Table 1:

Operating energy range	15 keV - 10 MeV
Continuum sensitivity, in photons cm^{-2} s^{-1} keV^{-1} (3σ detection, $\Delta E=E/2$, 10^5 s integration) *	2.3×10^{-6} @ 100 keV 1.6×10^{-6} @ 1 MeV
Line sensitivity, in photons cm^{-2} s^{-1} (3σ detection, 10^6 s integration)	1.8×10^{-5} @ 100 keV 3.8×10^{-4} @ 1MeV
Energy resolution (FWHM)	8% @ 100 keV 10% @ 1 MeV
Angular resolution (FWHM)	12'
Point source location accuracy (90% error radius)	30" @ 100 keV (50σ source) 3' @ 100 keV (5σ source) 5-10' @ 1 MeV (5σ source)
Timing accuracy	61 μs - 1 hr
Field of view	$8.3^o \times 8^o$ (fully coded) $29^o \times 29^o$ (zero response)

* Note that the continuum sensitivities given are statistical limits only, based on the in-flight measured background.

Imaging is performed using coded mask technology. There are two detectors operating simultaneously; the **I**ntegral **S**oft **G**amma-**R**ay **I**mager, ISGRI, a semi-conductor array optimised at lower energies, and the **PI**xellated Ceasium Iodide (**CsI**) **T**elescope, PICsIT, a crystal scintillator, for higher energies. The energy ranges covered by ISGRI and PICsIT overlap considerably; ISGRI covers the range 15 keV - 1 MeV; PICsIT covers 175 keV - 10 MeV. ISGRI is more efficient below about 200 keV (factor ~3); PICsIT is more efficient at higher energies (e.g., a factor ~3 at 511 keV), but the different background levels in the two detectors must also be factored into sensitivity calculations (as discussed in section V.3.3 and V.I.2).

Sections II.1, V.3 and Chapter VI of this document give the prospective observer a top-level description about the overall design and scientific capabilities of IBIS, to assist in the writing of observing proposals; we recommend these to be studied first.

The rest of Chapter II contains a more detailed engineering description of the instrument. Chapter III gives information about how IBIS actually works, while Chapter IV describes the scientific mode of the instrument. Finally, parts 1 and 2 of Chapter V describe the in-orbit behaviour of IBIS and how it is calibrated.

For more details we refer the interested reader to a sequence of papers on the IBIS payload in the A&A special INTEGRAL issue (2003, Vol. 411, L131-L229). This issue also contains various other papers on the first results from in-flight observations, including IBIS.

II. Description of the instrument

1. Overall design

IBIS is a gamma-ray imager operating in the energy range 15 keV to 10 MeV, with two simultaneously operating detectors covering the full energy range, located behind a Tungsten mask which provides the encoding.

The coded mask is optimised for high angular resolution. As diffraction is negligible at gamma-ray wavelengths, the angular resolution of a coded-mask telescope is limited by the spatial resolution of the detector array. The angular resolution of a coded mask telescope is defined by the ratio between the mask element size (in this case 11.2 mm) and the mask-to-detection plane distance (in this case 3.2 m). The IBIS detectors are made of a large number of small, fully independent detection units (pixels).

The detector features two layers, ISGRI and PICsIT: the first is made of Cadmium-Telluride (CdTe) solid-state detectors and the second of Caesium-Iodide (CsI) scintillator crystals. This configuration ensures a good broad line and continuum sensitivity over the wide spectral range covered by IBIS. The double-layer discrete-element design of IBIS allows the paths of interacting photons to be tracked in 3D if the event involves detection units of both ISGRI and PICsIT, if the event involves ISGRI and PICsIT triggers within 3.8 μs. The application of Compton reconstruction algorithms to these types of events (between a few hundred keV and a few MeV) allows in principle an increase in signal to noise ratio attainable by rejecting those events unlikely to correspond to source photons outside the field of view.

The detector aperture is restricted, in the hard X-ray part of the spectrum, by passive shielding covering the distance between mask and detector plane. An active Bismuth Germanate Oxide (BGO) scintillator VETO system shields the detector bottom as well as the four sides up to the bottom of ISGRI.

Figure 1 shows a cut-away drawing of the various components of IBIS (except the mask and the tube).

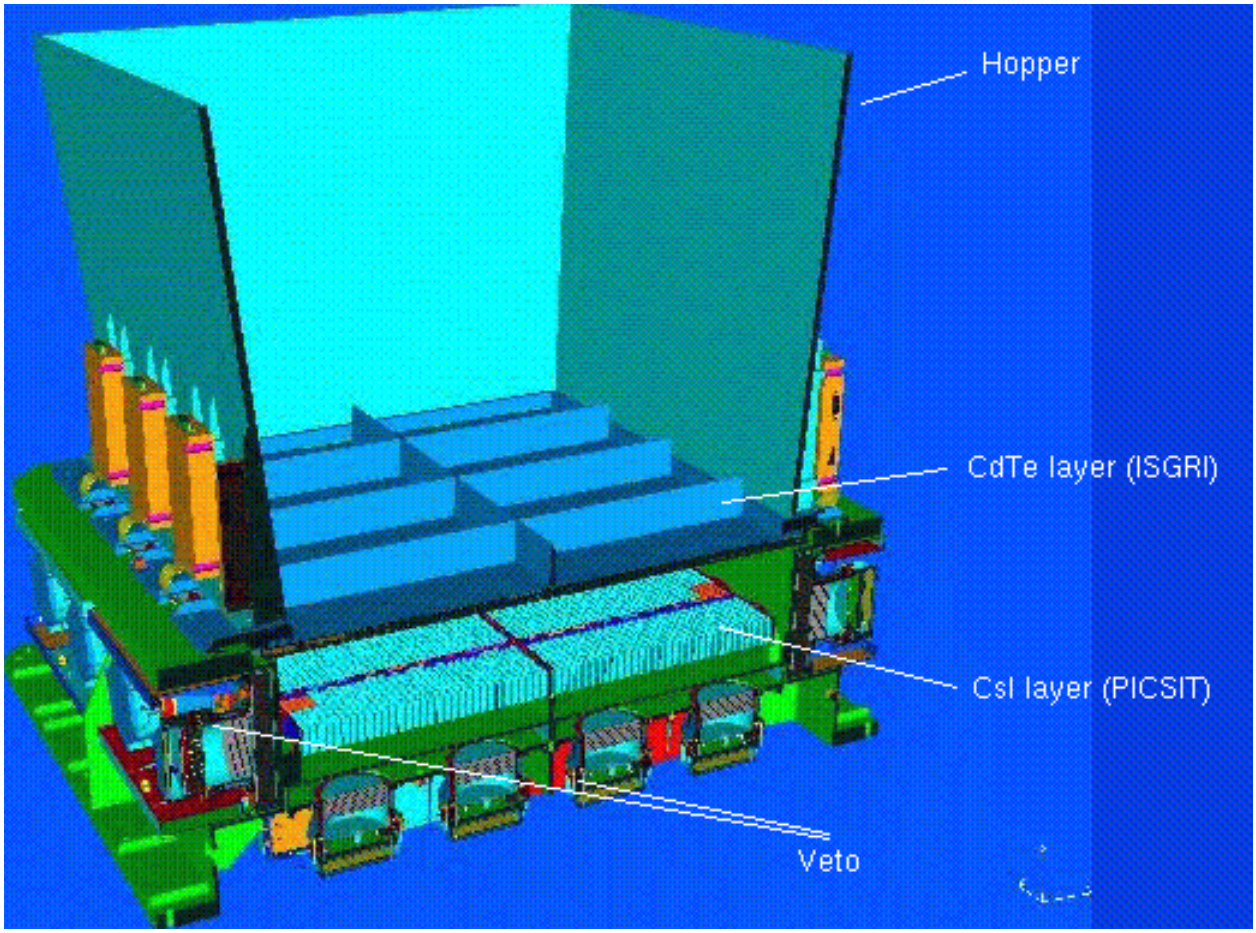

Figure 1. Cutaway drawing of the IBIS detector assembly, together with the lower part of the collimator ("Hopper"). The coded mask (not shown) is located 3.2 m above the ISGRI detector plane.

2. Imaging System

2.1 The Collimator

In order to maintain the low-energy response of IBIS when dithering (see the *Integral Manual*), the collimation baseline consists of a passive lateral shield that limits the solid angle (and therefore the cosmic gamma-ray background) viewed directly by the IBIS detector in the full field of view up to a few hundred keV.

The tube collimation system is implemented with three different devices:

The Hopper: Four inclined walls starting from the detector unit with a direct interface to the IBIS detector mechanical structure. The inclination of the hopper walls should ideally join the mask size, but the true inclination takes into account the presence of the Calibration System and the mechanical constraints. The hopper walls reach 550 mm out from the ISGRI top plane (850 mm from the PLM base), while the actual height is 530 mm. The shielding effect is obtained with Tungsten foils embedded in the four hopper walls. The hopper walls thickness is 1 mm. The hopper is not physically connected to the payload module structure.

The Tube: The Tube is formed by four payload module walls shielded with glued Lead foils. Two of the tube walls (-/+Z axis) are inclined (by 3.472 degrees to the vertical) in order to follow as closely as possible the inclined ideal tube shape, whilst the Y-axis walls are vertical, as shown in Figure 1. In particular the actual inclination of the Z walls is defined by the interface requirements with the hopper: the Z Tube walls stop at 20 mm in the horizontal plane from each upper edge of the hopper walls (i.e. at 850 mm from the Payload Module, PLM, base).

The mask side shielding: Four strips of 1 mm thick Tungsten provide shielding from the diffuse background in the gaps between the mask edges and the top of the tube walls.

2.2 The Mask Assembly

The IBIS Mask Assembly is rectangular with external dimensions of 1180 x 1142 x 114 mm^3, and consists of three main subsystems: the Coded Mask, the Support Panel and the Peripheral Frame with the necessary interface provisions.

The Coded Mask is square, of size 1064 x 1064 x 16 mm^3, made up of 95 x 95 individual square cells of size 11.2 x 11.2 mm^2.

The cells form a modified uniformly redundant array (MURA) coded pattern of 53 x 53 elements. Approximately half of the cells are opaque to photons in the operational energy range of the IBIS instrument, offering a 70% opacity at 1.5 MeV. The other half of the cells are open, i.e. with an off-axis transparency of 60% at 20 keV. Figure 2 shows the mask pattern.

The Support Panel includes those additional elements to support the mask, providing the necessary stiffness and strength to overcome the launch environment and the in-orbit operational temperatures.

The Peripheral Frame reinforces the sandwich panel and provides the mechanical interfaces with the INTEGRAL PLM.

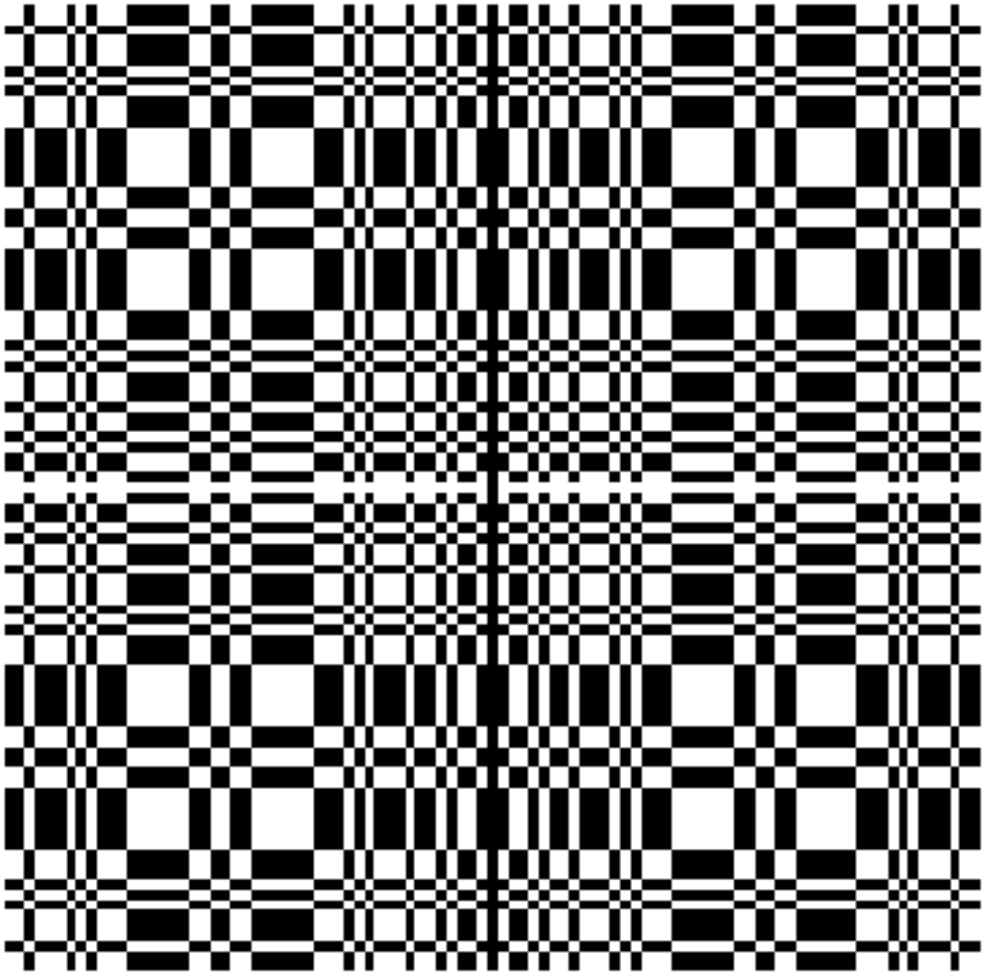

Figure 2. The IBIS coded mask pattern.

3. Detector assembly

The ISGRI and PICsIT detectors, both of which are situated 'under' the coded mask (and hence the astronomical source), are separated by 9 cm. PICsIT is situated below ISGRI.

3.1 Upper detector layer: ISGRI

Cadmium Telluride (CdTe) is a II-VI semi-conductor operating at an ambient temperature; 0^o +/- 20^o C is the optimum range. As CdTe detectors can be made to have a relatively small surface, they are ideally suited to build a pixellated imager with good spatial resolution. On the other

hand, their small thickness (necessary to achieve good energy resolution) restricts their use to the low energy domain (50% efficiency at 150 keV). Providing spectral performances intermediate between that attained by the cooled Germanium spectrometers (i.e., SPI) and those of the scintillators (i.e., PICsIT), the CdTe can be used well in the low energy domain (down to ~15 keV).

The CdTe layer is made of 8 identical Modular Detection Units (MDUs) each having 2048 pixels which are read out by 512 Application Specific Integrated Circuits (ASICs) (4 channels per ASIC). Each MDU is connected independently to a Detector Bias Box (DBB) and to a Module Control Electronics (MCE) system which ensures the A/D conversion and provides other on-board processing such as event filtering and active pixel monitoring.

The specifications are:

- Pixel (CdTe crystal) dimension: 4 x 4 mm^2, 2 mm thick
- Spacing between pixels: 600 μm (4.6 mm centre-to-centre)
- Minimum assembly: polycell of 16 pixels (4 x 4)
- MDU: 128 polycells (16 x 8)
- Layer: 8 MDUs (total of 8 x 64 x 32 pixels)
- Total sensitive area: 2621 cm^2 (16384 x 16 mm^2).

The CdTe layer is located at 294 mm above the PLM base plane and its overall thickness is about 15mm.

3.2 Lower detector layer: PICsIT

Caesium Iodide (CsI) is a I-VII scintillation crystal. The main characteristics of the layer are:

- Pixel (CsI(Tl)) crystal dimension: 8.55 x 8.55 mm^2, 30 mm thick
- Spacing between pixels: 550 μm (9.2 mm centre-to-centre)
- Minimum assembly (ASIC): 16 pixels (4 x 4)
- Module: 32 ASICs
- Layer: 8 Modules (total of 8 x 32 x 16 pixels)
- Total sensitive area: 2994 cm^2 (4096 x 73.1 mm^2).

The CsI(Tl) bars are optically bonded to custom-made low-leakage silicon PIN photodiodes. The design provides a high degree of modularity. The CsI(Tl) layer is divided in 8 rectangular modules of 512 detector elements, each module being integrated into a stand-alone testable subsystem. The CsI modules have the same cross-sectional shape as those of the CdTe.

4. Veto shield

The Veto shield is crucial to the operation of IBIS. IBIS uses anti-concidence logic to accept or reject detected events as real photons in the field of view, or background particles or photons propagating through, or induced in, the spacecraft.

The sides, up to the ISGRI bottom level, and rear of the stack of detector planes are surrounded by an active BGO Veto shield. Like the detector array, the Veto shield is modular in construction.

There are 8 lateral shields, i.e. 2 modules per side, and 8 bottom modules.

Each Veto Detector Module (VDM) includes:

- the BGO crystal and related housing
- two photomultiplier tubes (PMTs) optically coupled to the BGO and assembled with the dedicated Front End Amplifiers and high voltage (HV) divider
- one HV Power Supply
- one Veto Module Electronics box for Module control
- internal harness.

The high density and mean Z of the BGO ensure that a thickness of 20 mm is sufficient to reduce the detector background caused by leakage through the shielding of cosmic diffuse gamma–ray background and gamma–rays produced in the spacecraft, to less than the sum of all other background components.

5. Electronics

5.1 Analog Front End Electronics (AFEE)

Charge collection, signal filtering, and amplification are all performed by the Application Specific Integrated Circuits (ASICs) on both ISGRI and PICsIT. In ISGRI, the 16384 individual detector units (pixels) are grouped into 'polycells'. A polycell, the basic assembly unit of a detector module, is a hybrid circuit which receives a signal from 16 detectors via 4 ASICs.

5.2 Module Control Electronics (MCE) and PICsIT Electronic Box (PEB)

The MCE and PEB perform receipt, checking and execution of telecommands for ISGRI and PICsIT, respectively. They also collect and format the housekeeping data and process the analogue and digital data (energy and rise time). An important function of the MCE is to monitor the CdTe noise levels. In-flight a CdTe detector can become noisy and trigger the relevant MCE too

frequently, causing a large dead time with unacceptable loss of photons. Therefore the MCE monitors, in real time, the relative counting rates of each CdTe polycell. If a polycell exhibits noise, the MCE will, if necessary, switch it off (i.e., the pixel becomes 'disabled' or 'dead'). It can subsequently be reactivated and checked from the ground.

5.3 On-Board Calibration Unit

IBIS contains an on-board collimated radioactive ^{22}Na source. This allows regular calibration of PICsIT at both the 511 keV and 1275 keV lines (calibration to better than about 1% in 1-2 orbits). ISGRI can also use the 511 keV line, albeit at lower efficiency.

5.4 Digital Front End Electronics (DFEE) and 'FIFO'

The DFEE is situated behind the AFEE and processes the ASICs output for the 'first-in, first-out' (FIFO) data manager. FIFO sorts the events from different modules according to their true arrival time in the detector plane for transmission to the DPE/HEPI (see below). The DFEE also monitors the FIFO and instructs it when to send data to the DPE.

5.5 Data Processing Electronics (DPE) and Hardware Event Processor (HEPI)

The detector electronics chain ends at the DPE and the HEPI. The HEPI performs the data histogramming and generates the data structures for the DPE. The DPE handles all the interfaces between the instruments and the spacecraft for both uplink and downlink. For example, the packetting of data for the On-Board Data-Handling System before transmission to ground.

III. How the instrument works

Photons are detected in IBIS by several methods:

(i) Detection in ISGRI.

A photon is stopped in a single pixel of the semi-conductor, generating an electric pulse.

(ii) Detection in PICsIT.

A photon passes through ISGRI and is stopped in PICsIT, generating one or more scintillation flashes. PICsIT records detections which occur in just one pixel (single events), and detections which occur in more than one pixel (multiple events), separately.

(iii) Detection in both ISGRI and PICSIT (Compton mode).

Photons arriving in either ISGRI or PICsIT may produce secondary photons via Compton scattering and are subsequently detected in either layer. Note that the analysis of Compton events is not supported in the current Off-line Scientific Analysis (OSA) software, and are not taken into account in the instrument sensistivity calculations.

In Figure 3 we show the estimated efficiencies of the various detection techniques.

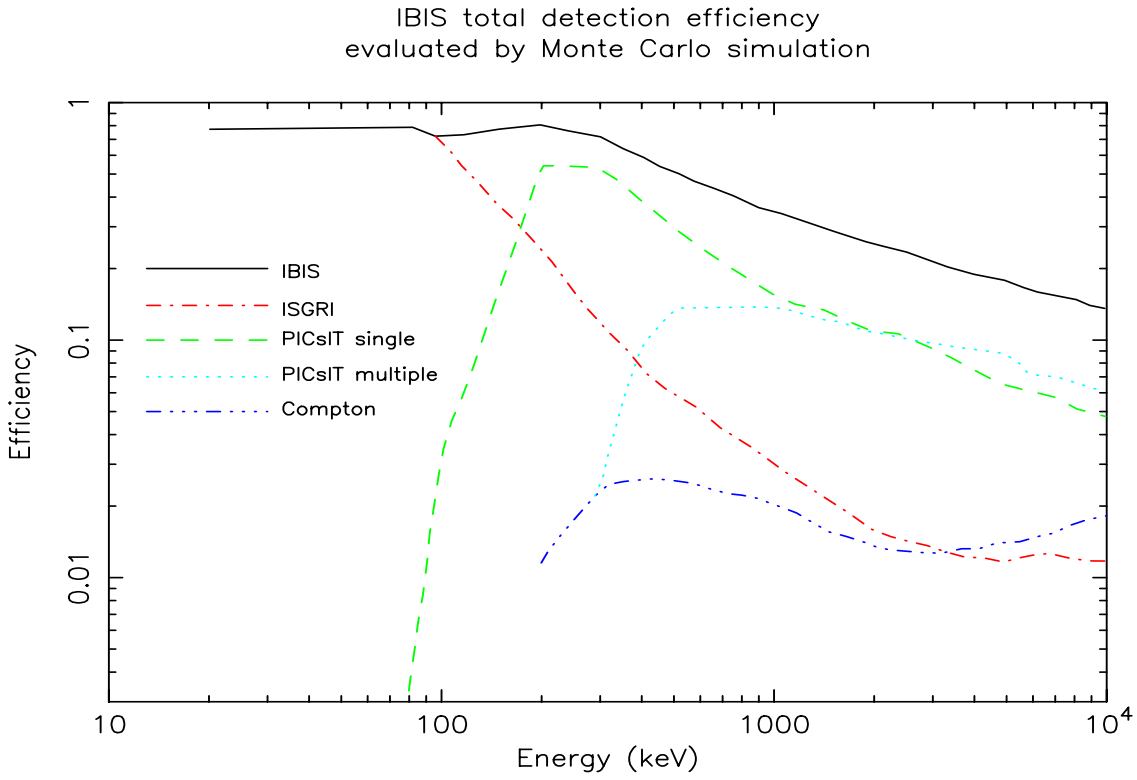

Figure 3. IBIS efficiencies for the various detection techniques, as evaluated pre-launch.

1. Imaging

Both ISGRI and PICsIT record the (x,y) coordinates of each event registered in the corresponding layer, to construct a shadowgram (a detector-plane image of the coded-mask shadow). The anti-concidence VETO is used to reject background events.

A photon detected in one pixel of a detection layer may be due to the background or to any celestial source visible from this pixel through the holes of the mask. It is therefore not possible to assign a given photon to a given source. On the other hand, cross-correlation techniques applied to a statistically significant ensemble of photons allow for a full reconstruction of the sources located in the fully coded field of view (FCFOV: 8.3˚ x 8˚). For the partially coded field of view (PCFOV: out to 29^o x 29^o) special cleaning techniques must be applied to the data for proper image reconstruction.

The actual sky coverage during an observation depends on the dither pattern. For example, during a 5 x 5 dither pattern a 36.3^o x 36^o field is imaged out to zero response, while a 16.3^o x 16^o region is sampled (at least partly) with full coding.

2. Spectroscopy

2.1 Detection in ISGRI

In principle, the amplitude of the pulse yields the energy of the incident photon. However, above 50 keV the energy determined is a function of the pulse height and rise time, so both must be used to determine the energy of the incident photon. In addition, the resulting line profile (energy resolution) is no longer Gaussian, but more similar to a Lorentzian. The energy resolution depends on the operating temperature, and also on the bias voltage; the bias voltage has to be optimised as a trade-off between high resolution but more noise (high voltage) or lower noise but lower resolution (low voltage).

2.2 Detection in PICsIT

The energy of the incident photon is derived, in each crystal bar, from the intensity of the flash recorded in the photodiode. For multiple events it is derived by summing the energies derived from the intensity of each of the flashes. The energy resolution of PICsIT is a function of the signal-to-noise of the events, the electronic noise at low energies, and the light output.

2.3 Compton events

For Compton events the energy is determined from the sum of energies for the initial event and the scattered photon. Note again that the analysis of Compton events is currently not supported.

3. Timing

The ISGRI time resolution is 62 μs for each detected event. PICsIT spectra and images are accumulated every 1800-3600 seconds depending on the (flexible) dithering time; a spectrum alone (but with low resolution - from two to eight energy channels) is available every several milliseconds. See also Chapter IV.

4. Polarimetry

In principle, the multiple events in adjacent PICsIT cells can be used to determine the polarisation of the incident photons, because of the Klein-Nishina cross-section with polarisation angle. However, at present polarisation studies are not feasible, and it is, therefore, not offered in this AO.

IV. Overview of observing modes and parameters

IBIS has several observing modes, for engineering and calibration purposes. However, for scientific use there is only one operating mode, i.e. Science Mode. The Science Mode has no user-selectable parameters.

In Science Mode, ISGRI registers and transmits events on a photon-by-photon basis, i.e. every event is tagged with its (x,y) position on the detector plane, event energy (from the pulse height and rise time) and event time.

PICsIT, in principle, can also operate in photon-by-photon mode. However, given the higher background compared to ISGRI, with the available telemetry there would be unacceptable data losses. Therefore, the standard mode for PICsIT is 'histogram'. Images and spectra (full spatial resolution, 256 energy channels) are accumulated for 1800-3600 seconds (depending on the flexible dithering time) before transmission to ground. There is no time-tagging internal to the histogram, i.e. spectral imaging has a time resolution of 1800-3600 seconds only.

Additionally, coarse spectra without imaging information are accumulated by PICsIT and transmitted with far higher time resolution. However, without imaging information their usefulness is limited to observations of very strong sources where the source count rate dominates the background. The time resolution and the number of energy channels for this spectral timing data can be set from the ground. The time resolution can take values between 0.976 ms to 500 ms. The currently used values are 3.9 ms and 4 energy channels (i.e., 156-208 keV, 208-260 keV, 260-364 keV and 364-676 keV).

V. Performance of the instrument

1. Components and sources of instrumental background

For most astronomical sources, the background will be higher than the measured source intensity.

The principal sources of background in IBIS are:

- for ISGRI at low energies (up to about 100 keV), the fluorescence emission of the passive shield elements and the diffuse cosmic gamma-ray background;

- for ISGRI at higher energies, and for PICsIT, the radioactive decay of unstable nuclei created by the spallation interactions of cosmic-ray protons and their secondary particles in the massive parts of INTEGRAL.

Other effects which influence the background are, e.g., solar activity and VETO performance. The particle background varies over the solar cycle. It is lowest at solar maximum, when the higher solar magnetic field inhibits the propagation of cosmic rays into the inner solar system. It is expected to be a factor of ~2 higher at solar minimum.

The reduction in count rates compared to the no-VETO case has been evaluated during the PV phase to be of the order of about 50% for the low energy detector, ISGRI, and about 40% for PICsIT. The actual Veto configuration has been optimised to give the best uniformity of Veto operation.

Typical in-flight background spectra as observed by ISGRI and PICsIT are shown in Figure 4. The observed background rates compared to the Crab on-axis count rates are given in Table 2. The background rates quoted here are determined in-flight using calibration observations.

The (background) detector images are strongly structured (apart from dead pixels, see next Section). They have been evaluated in order to be taken into account in the background subtraction algorithms. Currently, sets of background maps with long integration times (up to 1.7 Ms) are included by default in the Off-line Scientific Analysis (OSA) software, version 4. These maps optimize background subtraction and allow to reach higher signal-to-noise in the detections.

Already since the first instrument activation, frequent bursts of counts in the PICsIT count rate have been observed. In the accumulated detector images they are seen as tracks of bright pixels; they indicate that these events are related to the interaction of cosmic rays with the detector. The contribution of these cosmic-ray induced triggers to the total PICsIT background is of the order of 10%. However, these triggers are mainly effective at low energy channels, i.e., below ~300 keV (up to about 30% of the total background).

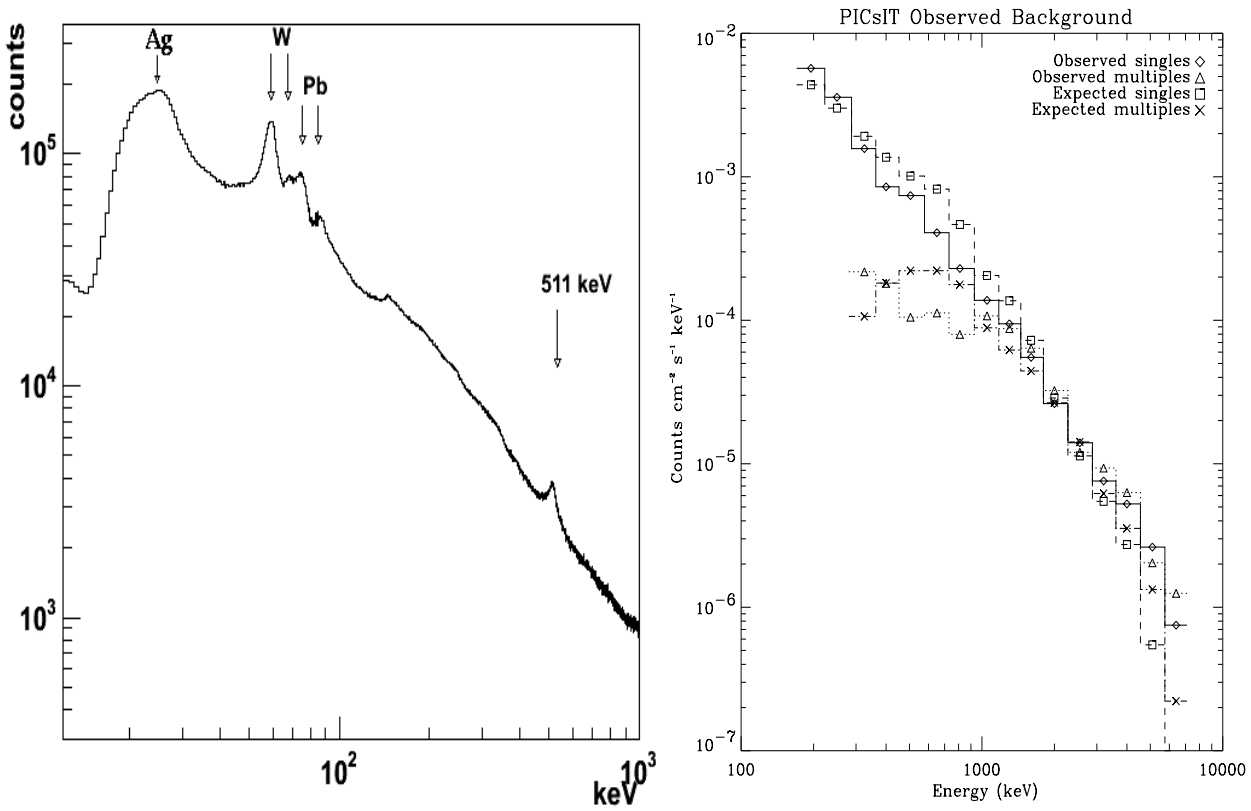

Figure 4. In-orbit background spectra for ISGRI (*left*) and PICsIT (*right*). The ISGRI and PICsIT spectra are from empty field observations in revolution 96 (effective exposure time 36.4 ksec) and in revolution 38, respectively. For ISGRI the contribution from lines from different instrument components are indicated. For PICsIT the spectrum for single and multiple events is compared with the expected spectrum obtained from MonteCarlo simulations.

Table 2: Background rates compared to the Crab rates

Instrument	Background (Solar Max) cts s^{-1}	Crab on-axis cts s^{-1}
ISGRI	600	220
PICsIT	3650	7.7

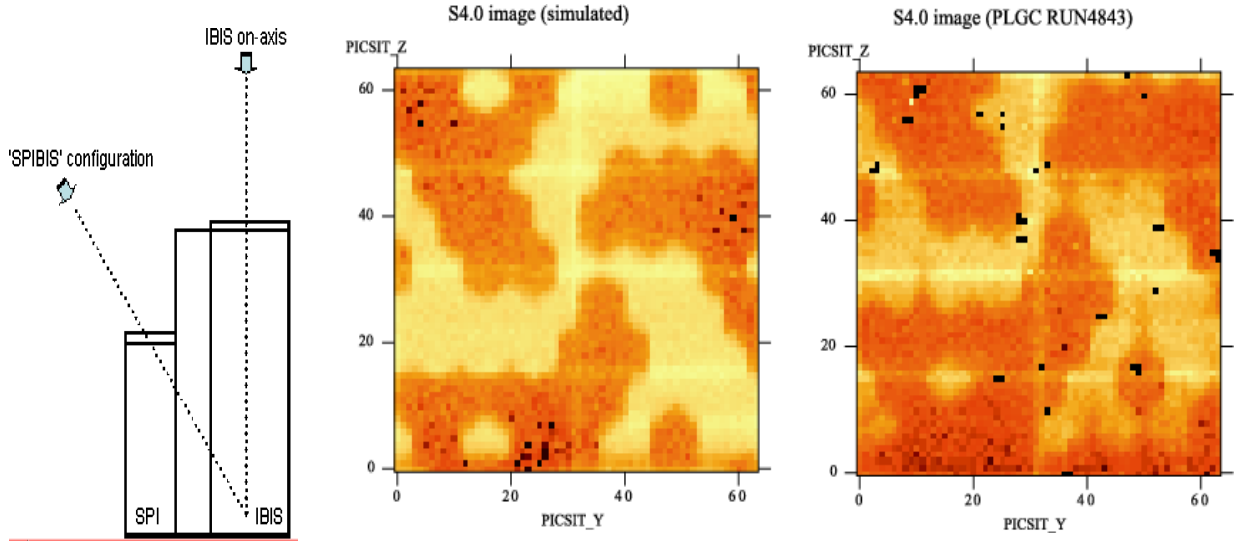

Figure 5. ***Left:*** **Off-axis source positions for the SPIBIS configuration, as well as the shielding tests, during the pre-flight calibrations.** ***Middle and right:*** **PICsIT shadowgrams from simulations (*middle*) and pre-flight calibration data (*right*). The images are slightly offset due to the inaccuracy in the supplied source position.**

IBIS is located next to SPI and JEM-X (see the *Integral Manual*), which are also coded-mask telescopes. Since gamma-rays are highly penetrating, it is possible for them to pass through parts of the spacecraft or instrument structures, as well as coded masks and to be detected by the gamma-ray instruments. Therefore, off-axis gamma-rays (effectively those with energies above ~300 keV) that pass through either the SPI or the JEM-X coded masks may cast a shadow of this mask onto the IBIS detectors (see Figure 5). The former combination is often referred to as the ''SPIBIS'' instrument. Although it effectively increases the field of view of IBIS, a bright gamma-ray source would thus add additional counts and modulation to the IBIS histogram, which considerably complicates the image reconstruction.

The SPIBIS effect has been calibrated before launch. Currently, the ISOC avoids scheduling sources when either of the three brightest sources/regions, i.e., Crab, Cyg X-1 or the Galactic Center region, are visible by IBIS through the SPI mask. This ensures that the observation is uncontaminated by a possible SPIBIS effect.

2. Instrumental characterisation and calibration

The ISGRI and PICsIT detectors were, and still are, calibrated in-orbit. At present the calibration is good up to the 10% level. This means that in the spectral fits the deviations between the observed spectrum and actual model are within 10%. Observations of the Crab nebula and pulsar are performed, to enable regular verification of the detector uniformity and its energy response, as well as enhancing the calibration. As an example, Figure 6 displays an ISGRI Crab calibration spectrum, showing the status of the calibration.

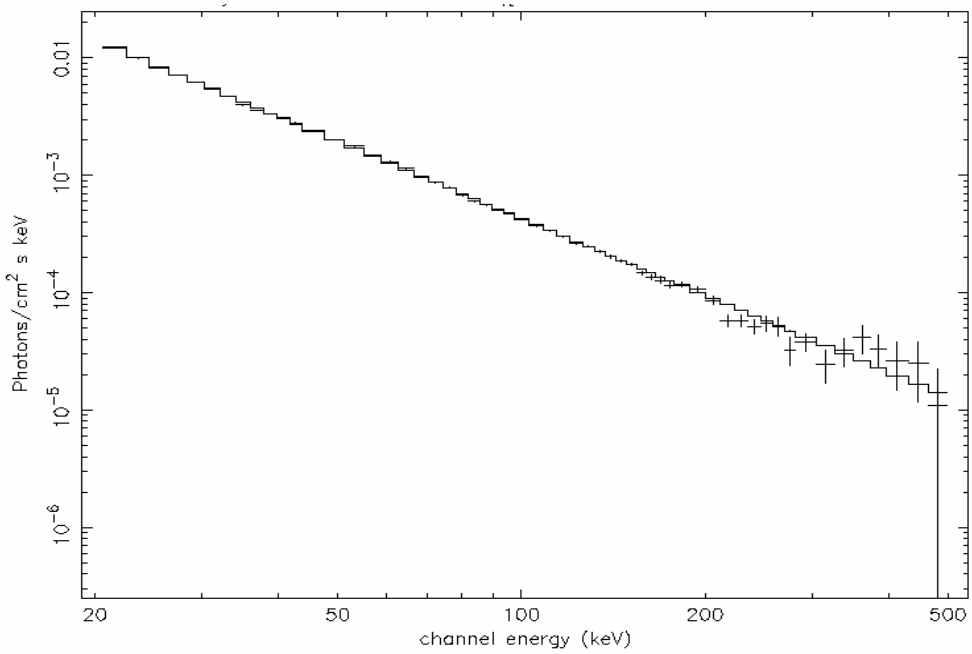

Figure 6. Crab photon spectrum together with the fit to a power-law emission model, dN/dE= 0.44x10^{-3} (E/100 keV)$^{-2.17}$ photons cm^{-2} s^{-1} keV^{-1}. Based on ISGRI data collected during an on-axis staring observation in revolutions 102 and 103, with a total observation time of 50 ksec. The data was analysed using OSA version 4, and a systematic error of ~2% has been added to each spectral bin. The goodness-of-fit is χ^2 = 66 for 55 degrees of freedom.

The instrument characteristics will also be checked after strong disturbing events such as solar flares. The energy response and spectral resolution are monitored on long time-scales using the de-excitation lines at 511 keV and 1275 keV emitted by the on-board ^{22}Na calibration source, and at 59.3 keV using the background-induced Tungsten fluorescence line from the coded mask and hopper walls.

ISGRI shows a loss of gain of about 3% per year. The data analysis software therefore contains a time-dependent gain correction for ISGRI. Taking into account the expected PICsIT gain variation of 0.3%/^{o}C measured during on-ground thermal tests, the average gain (over the whole detection plane) measured in-flight indicates that the PICsIT temperature gradient along the INTEGRAL orbit is the dominant factor in the observed PICsIT gain variation.

At high energies (typically > 1 MeV), the background so strongly dominates the flux of any calibration source that a large amount of data is needed. It was not possible to take sufficient measurements in the few weeks of the commissioning phase. Therefore, data accumulated through the routine operations phase are used to extend the calibration into the MeV region.

The current number of disabled (or 'dead') pixels for ISGRI is ~500 (of a total of 16384 pixels). For PICsIT the current number of disabled pixels is stable at ~53 (of a total of 4096 pixels).

3. Measured performance

3.1 Imaging resolution

In the FCFOV the off-axis response (sensitivity, spatial resolution) is fairly uniform, at least above ~30 keV (at the lowest energies the off-axis transparency of the mask falls off quickly). However if a 5 x 5 dither pattern is used there is a slight (~2%) loss in overall sensitivity averaged over the dither pattern.

The angular resolution of IBIS is 12' FWHM. However a feature of the mask is that the centroiding accuracy for a point source can be much finer. Figure 7 shows the measured point source location accuracy (PSLA) in ISGRI as a function of signal-to-noise ratio from observations (points) and theory (line). The absolute localisation (after misalignment correction) is better than 1-1.5' for bright sources. The PICsIT PSLA is a factor ~2 coarser than that of ISGRI (see Figure 8).

Observers should keep in mind that when INTEGRAL is performing staring observations, clear residual systematic structures are seen in the reconstructed sky images that can degrade the science objectives. It is therefore advised to use one of the dithering modes. We also note that if a strong source (such as the Crab) is present in the partially coded field of view, so-called ghosts may appear in the reconstructed sky images. In these cases we recommend to use, if possible, a different pointing so that the contaminating source falls outside the partially coded field of view.

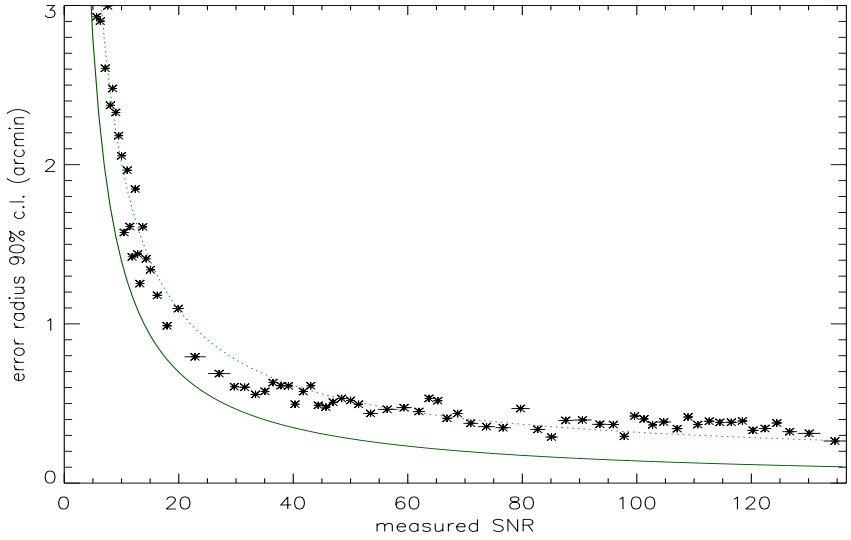

Figure 7. The point-source location accuracy (PSLA; 90% confidence level accuracy) as a function of the measured source signal-to-noise ratio for ISGRI using in-flight calibration observations. The expected curve (continuous line) is also shown. The dotted line shows the fit to the data points.

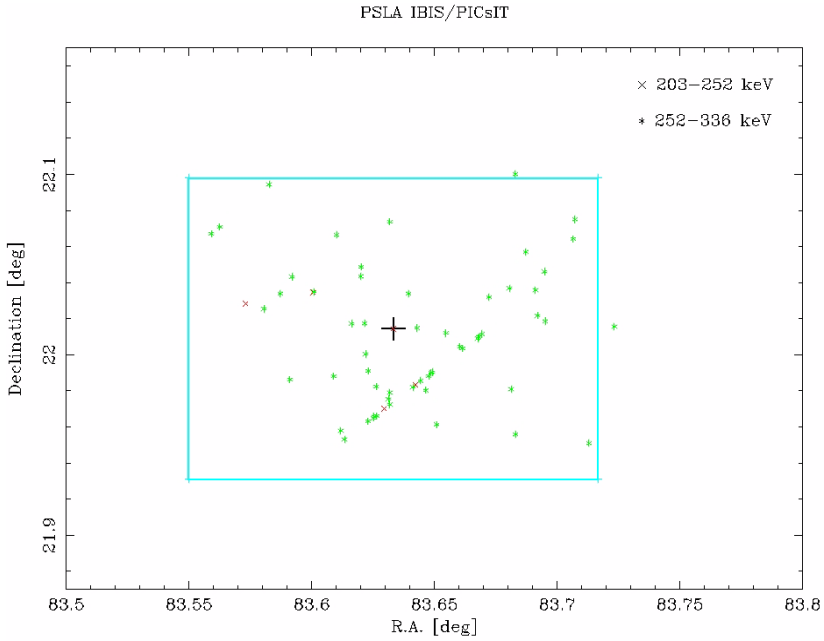

Figure 8. The point-source location accuracy (PSLA) for PICsIT using Crab observations from revolutions 39, 43, 44 and 45. Results for 2 energy bands are given (203-252 keV and 252-336 keV). Only detections with at least 3σ per science window (or exposure) are used. The central large cross indicates the catalog position of the Crab, and the rectangle around it represents the dimension of one pixel of PICsIT (10' size).

3.2 Spectral resolution

The spectral resolution of ISGRI has been measured during pre-flight tests on the engineering model, as well as in-flight (Figure 9). Resolutions of 9% at 60 keV (W fluorescence) and 4.6% at 511 keV have been measured from in-flight spectra. These results are in perfect agreement with the pre-flight measurements and show the stability of the instrument, even after disturbing events such as solar flares. Figure 10 shows the PICsIT spectral resolution, as determined in-flight. The in-flight data do not show any degradation or changes in the PICsIT spectral performance so far.

3.3 Sensitivity

The full calculations for continuum and line sensitivities are in principle given by the following equations:

V-3.3.1 Continuum:

$$S_c = n_\sigma \, [TA\Delta E \, \varepsilon_T \varepsilon_I \, (\vartheta_o - \vartheta_c)^2]^{-1} \{ n_\sigma (\vartheta_o + \vartheta_c)^2 + [n_\sigma^{\,2} (\vartheta_o - \vartheta_c)^2 + 4(\vartheta_o - \vartheta_c)^2 \, T\Delta E \, AB]^{0.5} \}$$

V-3.3.2 (Narrow) line:

$$S_l = n_\sigma \, [TA\varepsilon_p \varepsilon_I \, (\vartheta_o - \vartheta_c)^2]^{-1} - \{ n_\sigma (\vartheta_o + \vartheta_c)^2 + [n_\sigma^{\,2} (\vartheta_o - \vartheta_c)^2 + 4(\vartheta_o - \vartheta_c)^2 \, T\delta E \, AB]^{0.5} \},$$

where:
- S_c is the continuum sensitivity in photons cm^{-2} sec^{-1} keV^{-1},
- S_l is the line sensitivity in photons cm^{-2} sec^{-1},
- n_σ is the number of sigma,
- ΔE is the energy bin (for continuum),
- δE is the energy resolution,
- A is the detector area,
- ε_p, ε_T are the peak and total efficiencies,
- ε_I is the imaging efficiency, a function of the coding noise and dither pattern,
- B is the background countrate in counts cm^{-2} sec^{-1} keV^{-1},
- ϑ_o, ϑ_c are the open and closed mask element transparencies, and
- T is the observation duration.

Note that for a broad line with a FWHM of ΔE keV, the sensitivity is reduced by $(\Delta E/\delta E)^{1/2}$.

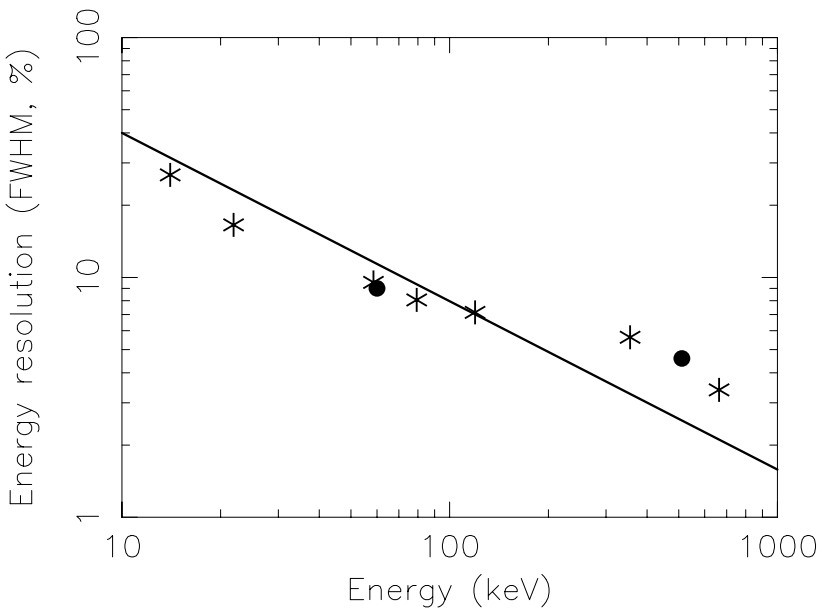

Figure 9. The energy resolution of ISGRI. Solid line: theoretically expected values; points (stars): values measured before launch using an engineering model. The study of the in-flight W fluorescence line at 60 keV and the e^+e^- annihilation lines at 511 keV (shown as filled circles) do not reveal any evidence of a change of the ISGRI spectral performance.

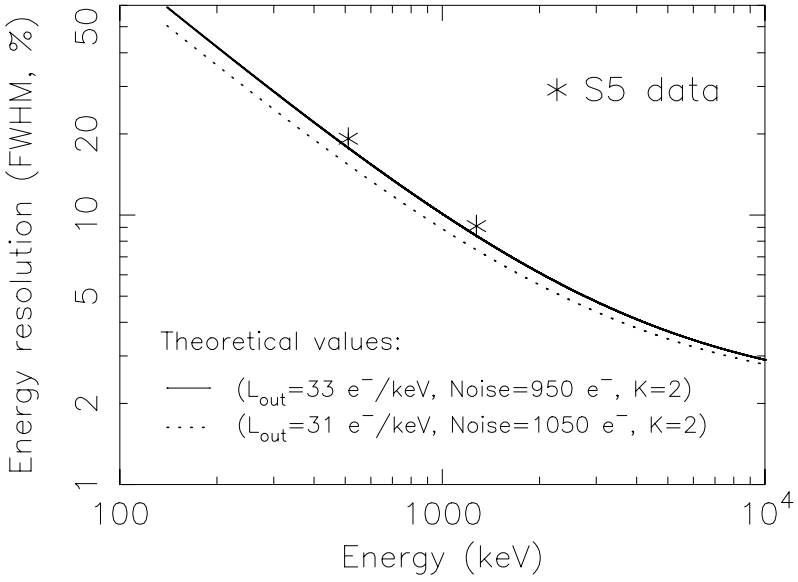

Figure 10. PICsIT energy resolution at 511 and 1275 keV as measured in-flight using Calibration Unit (S5) data (shown as stars). Also shown are the theoretical expectations as determined from pre-flight tests using an engineering model. The electronic-noise values ("Noise") refer to one ASIC only; a 10% increase is expected when extrapolating to the complete detector electronic chain.

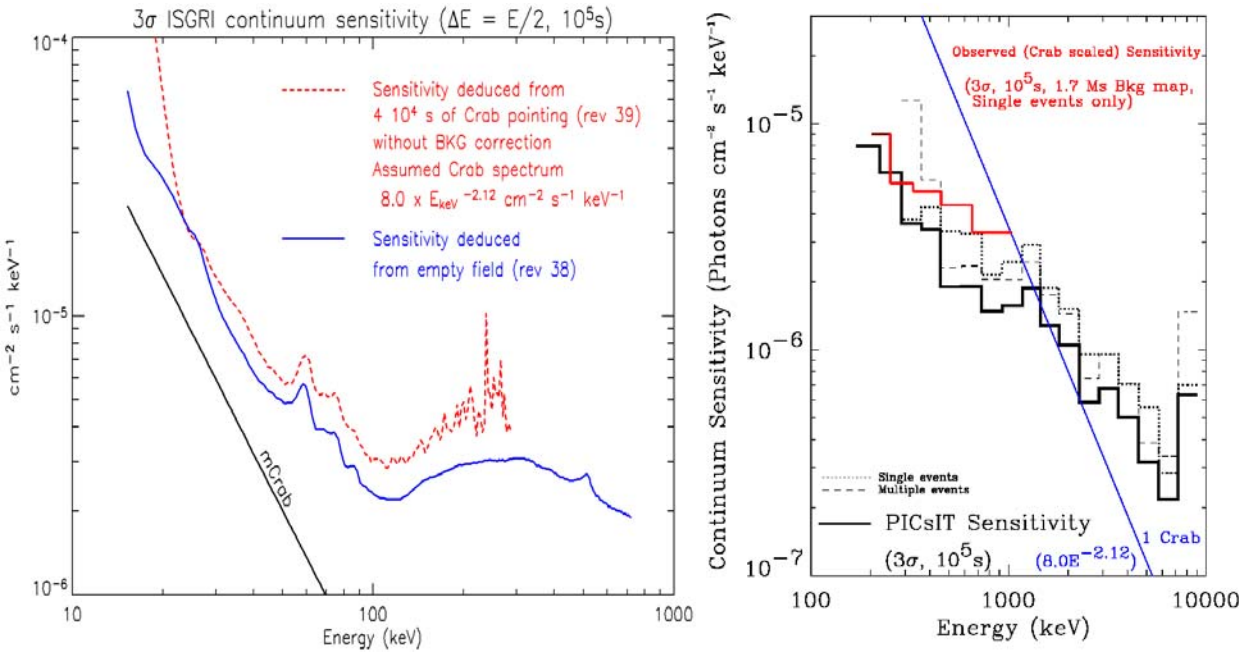

Figure 11. ***Left:*** **ISGRI statistically limited continuum sensitivity (blue curve) deduced from an empty field observation, compared with the sensitivity deduced from the Crab observations,** ***without*** **background corrections.** ***Right:*** **PICsIT statistically limited continuum sensitivity (black histograms; shown are single and multiple events separately, as well as combined), scaled to the in-flight background count rate, compared with the sensitivity obtained by scaling from the Crab observation using OSA software version 4 (red curve; single events only). Both ISGRI and PICsIT continuum sensitivities are for a 10^5 s exposure, 3σ detection and continuum binned to ΔE= E/2.**

The ISGRI and PICsIT broad-band statistically limited ('calculated') sensitivity curves, as well as the sensitivities deduced from Crab observations are shown in Figure 11**.** The calculated sensitivity curves of ISGRI and PICsIT are compared in Figure 17 in Chapter VI. The statistically limited line sensitivities are also shown in Chapter VI (Figure 18). In Chapter VI we explain how the sensitivites may be used to estimate signal-to-noise ratios and observing times. Note that the calculated sensitivities are applicable for a clear field with perfect uniformity and background correction. The observed and calculated sensitivities agree within a factor of ~2, see Figure 11. Part of this is related to systematics which increase in importance in fields with large exposure times and large number of sources. The latter is of importance at 20-150 keV; at higher energies there are not many bright sources. The systematics start to dominate for exposures times longer than several 100 ksec. We stronly recommend the final proposed times always to be calculated using the on-line observing time estimator (OTE); those are the only values which will be used in the technical feasibility check of the proposal performed for the Time Allocation Committee (TAC) by the ISOC. OTE uses the statistically limited sensitivity curves.

PLEASE NOTE: the continuum sensitivities shown here and given in Chapter VI are for ***monochromatic flux density (photons cm^{-2} s^{-1} keV^{-1})***, while the input for the observing time estimator (OTE) is in ***broad-band flux (photons cm^{-2} s^{-1})*** within a user-defined energy range.

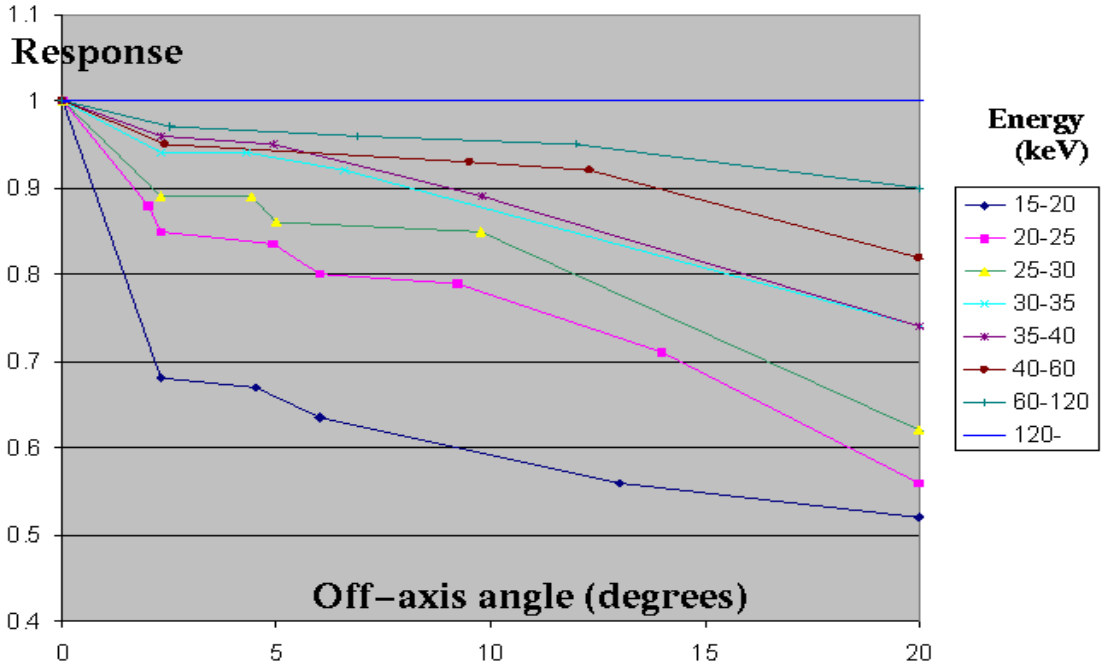

Figure 12. Deviations from the theoretical response of the IBIS telescope for various off-axis angles in different energy bands. Note that the OSA software version 4 corrects for these deviations.

3.4 Off-axis instrument response

The off-axis response of the IBIS telescope has been characterized during the Crab calibration observations in early March 2004. Users employing the OSA software version 3 should be aware that the flux of off-axis sources can be reduced by up to 50% in the FOV at low energies (around 20 keV) as shown in Figure 12. Corrections to both images and spectra for off-axis sources are included in the OSA software version 4, and these reduce any remaining off-axis effects to less than 10%. Residual effects due to azimuthal dependence on the mask transmission are under investigation and may be corrected in future OSA software releases.

3.5 Timing capabilities

The *time resolution* in ISGRI is 61 μs. For PICsIT, imaging and spectral histograms are collected every 1800-3600 seconds (depending on the flexible dithering time) - there is no finer time resolution available inside the histogram. The spectral timing data of PICsIT (no imaging!) will be accumulated every few ms; the resolution can be selected from ground and can take a value between 0.976 and 500 ms. The value used in routine operations is currently 3.9 ms. Once selected, it will apply to all PICsIT observations.

The *absolute timing accuracy,* i.e., the barycentric correction to event times measured in IBIS, depends on not just the time resolution, but also on time frame synchronisation in the instrument and spacecraft subsystems, and the uncertainty in the spacecraft position around the orbit. Calculations indicated a 1σ uncertainty of 61 μs and 3σ uncertainty of 92 μs. Based on in-flight observations, the relative timing between the INTEGRAL instruments can be reconstructed within 10 μs, whereas the absolute timing accuracy is about 40 μs. A more accurate calibration might be performed via dedicated millisecond pulsar observations.

The dead-time in ISGRI is mainly due to encoding the events and to the coincidence applied with PICsIT, VETO and the calibration source. It amounts to about 24%. For PICsIT the overall dead-time amounts to about 5-6%.

VI. Observation "Cook book"

1. Astronomical considerations on the use of the instrument

In this section we present some typical examples of the kinds of scientific studies suitable for IBIS, with some illustrative results obtained in-flight. The selection is by no means exhaustive.

Black Holes

IBIS can detect all currently known persistent black-hole (BH) candidates in our galaxy. Examples are GRS 1758-258 and 1E 1740.7-2942, see Figure 13.

IBIS is used to investigate whether BH binary systems are characterised by distinctive X/γ-ray signatures. For example, are their spectra significantly harder than those from neutron star systems - is the bulk of their luminosity indeed in the soft gamma–ray band? Can the spectral turnover be measured and the total luminosity constrained?

IBIS is also able to detect any Galactic hard X/gamma–ray transient in outburst within the few minutes exposures provided by the routine Galactic Plane Survey (GPS), and the pointings around the Galatic Centre and the Galactic spiral arms (see the *Guaranteed Time* document). Subsequent follow-up longer observations can monitor the light curve of the transient, its spectral evolution, and possible transient lines with unprecedented spectroscopic quality. So far IBIS has been able to detect about 30 new transients within the AO-1 and AO-2 Core Program investigations and about 10 during Open Time observations. Furthermore, transients in outburst, such as IGR J17464-3213/H1743-322 and GX 339-4, as well as state transitions, have been seen.

Of particular interest in such transients is the appearance of broad transient lines. For example, Nova Muscae 1991 (GS 1124-68) showed a broad line at 480 keV - redshifted annihilation? - and another spectral feature near 200 keV, possibly due to Compton backscattering. IBIS will measure such features with good statistical accuracy on timescales of hours, allowing the study of the rapidly changing geometry and physical conditions in the immediate vicinity of black hole systems.

It is worthwhile to mention the at least 17 'classical' X-ray sources have been detected at energies greater that 20 keV with high statistical significances, clearly demonstrating the IBIS foreseen capabilities and the key strategic value of the regular survey of the Galactic plane and the pointings towards the Galactic arms.

Neutron Stars

Neutron stars (NS) - both in binary systems and isolated NS (e.g., pulsars) - are objects of prime interest for IBIS.

For example, observations of the Galactic Centre region with SIGMA, BeppoSAX and RXTE indicate that X-ray bursters are a newly identified class of soft gamma-ray sources.

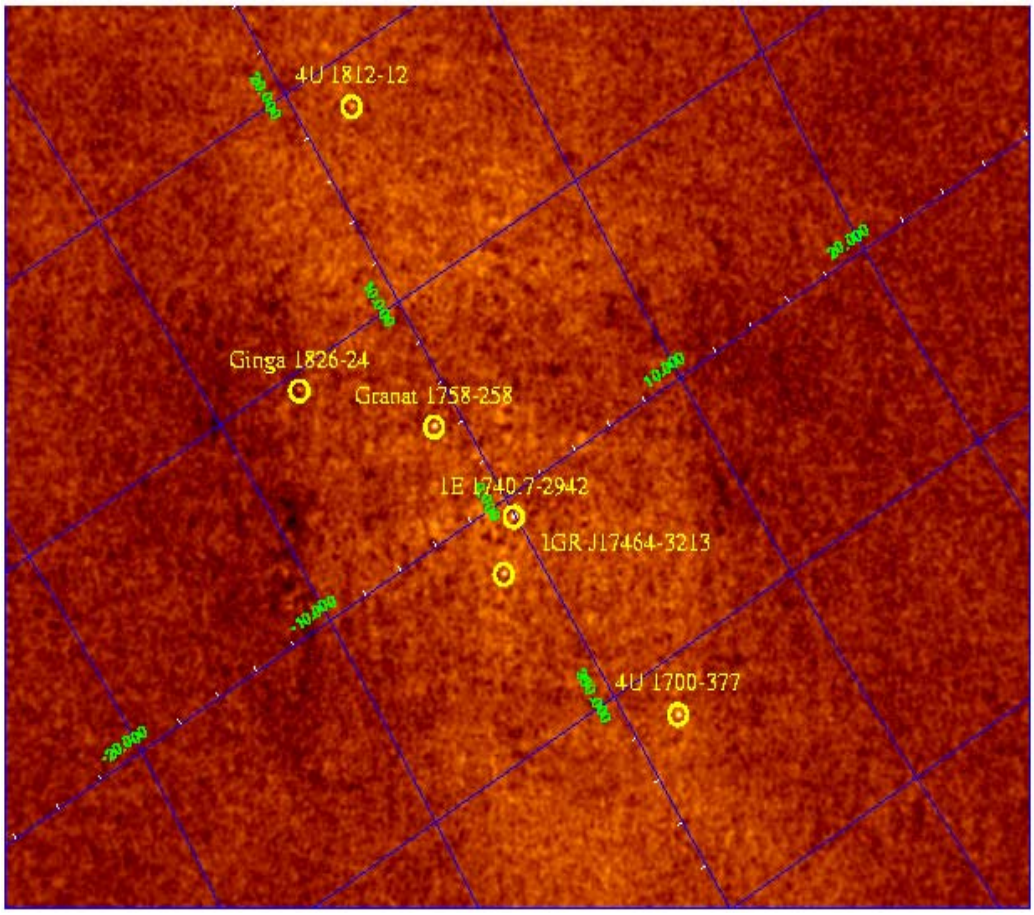

Figure 13. ISGRI mosaic sky image of the Galactic Center region in the 120-250 keV energy band. In this hard X-ray band 6 sources are clearly detected, i.e., 2 neutron-star LMXBs (GS 1826-238 and 4U 1812-12), 3 black-hole LMXBs (GRS 1758-258, 1E 1740.7-2942 and IGR J17464-3212/H1743-322 and 1 neutron-star or black-hole HMXB (4U 1700-377). Data are from the AO-1 Galactic Center Deep Exposure (GCDE) taken between revolutions 46 and 123, for a total of about 1.5 Msec.

About 20 X-ray burst sources have now been seen by IBIS at energies greater than 20 keV, and many of them up to at least 100 keV. Figure 14 shows an example of 2 X-ray burst sources as seen in four energy bands (see also Figure 13 for a detection at even higher energies).

The good spectral resolution and large collecting area of IBIS at low energy will enable the study of cyclotron lines from magnetized NS in great detail, e.g., phase-resolved line shapes/ widths.

The good sensitivity at higher energy will allow detection of isolated pulsars in the MeV region, where their properties are so far poorly measured.

It is worth noting in general that the soft gamma-ray domain is probably the best region to "see" the accretion at work close to the compact object.

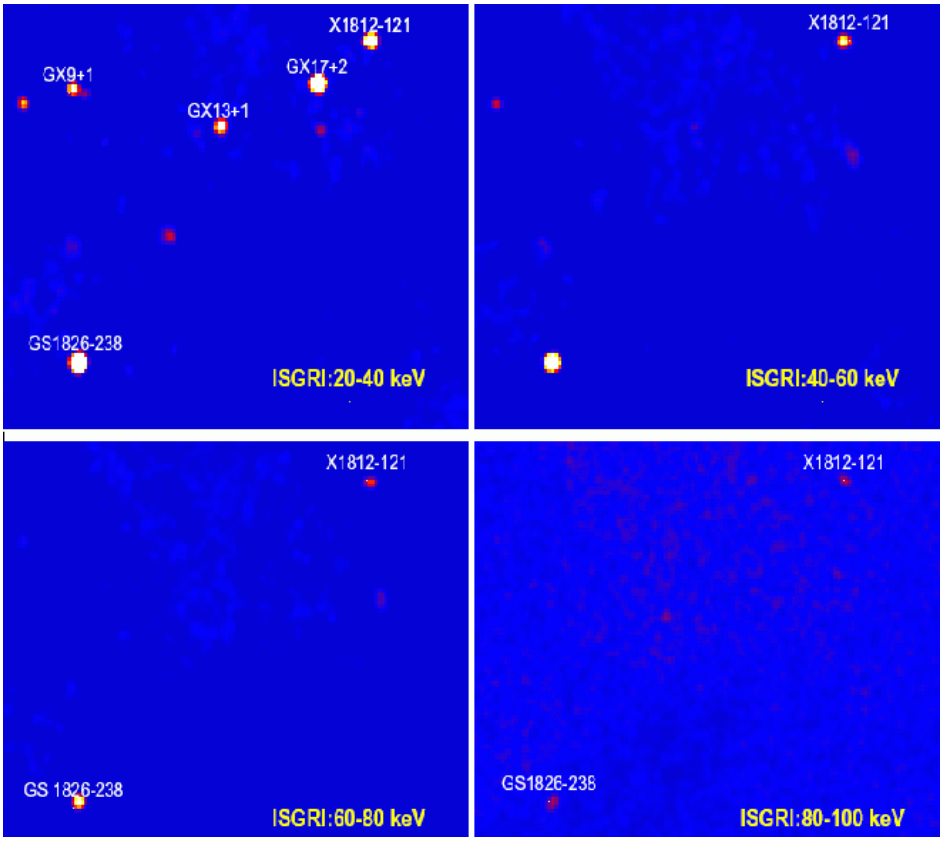

Figure 14. Example of ISGRI sky images in 4 energy bands. The sky region includes 2 X-ray bursters, which are seen up to ~100 keV.

Supernovae

In most cases, the line sensitivity of IBIS is independent of the intrinsic line width and IBIS provides a powerful imaging complement to SPI - studying the spatial distribution of hot-spot line emission from supernova remnants and in the galactic plane in general, while SPI provides fine spectroscopy. Also, hidden young SNR will show up as emission-line point sources.

Extragalactic studies

A main result of CGRO and BeppoSAX observations of AGN is that their broad-band continua strongly depends on their AGN type.

At *low energies* these will be mostly Seyferts. Although it is known that their spectra fall off somewhere above ~50 keV (but below ~1 MeV), the details of this cut-off are still highly uncertain, mainly due to difficulties in fitting complex models over a limited (due to the lack of sensitive high-energy observations) energy band. Another intriguing issue which IBIS will address is whether there is a large population of Compton-thick AGN visible above 30 keV.

At *higher energies* most of the sources will likely be blazars, whether MeV peaked or TeV peaked. The main interest with INTEGRAL is the determination of the spectral characteristics from keV to MeV energies (spectral breaks? hard tails?).

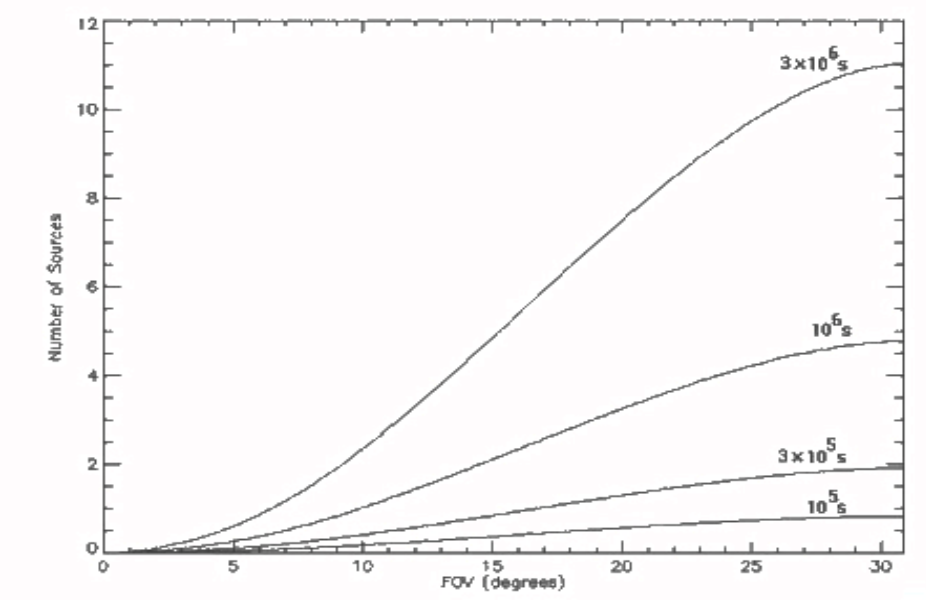

Figure 15. Number of sources visible (per square degrees) above a given flux limit in the 13-80 keV band (based on results obtained from HEAO-1 A4 and BeppoSAX/PDS) taking into account the IBIS sensitivity and FOV, for different exposure times.

IBIS survey

From the IBIS survey it is estimated that a 1 mCrab source in a 1 Ms observation provides a 5σ detection (20-100 keV), assuming negligible systematic errors as normally observed for extragalactic fields. This correspond to a flux of $2x10^{-11}$ erg cm^{-2} s^{-1} in the 13-80 keV band. Figure 15 shows the result of convolving the number of sources visible (per square degrees) above a given flux limit in the 13-80 keV band (based on results obtained from HEAO-1 A4 and BeppoSAX/PDS) taking into account the IBIS sensitivity and FOV, for a 10^5, $3x10^5$, 10^6 and $3x10^6$ s observation, respectively. We expect typically 3 (5) AGN detected above the 5σ level in a 500 (1000) ks exposure over the entire field of view of IBIS.

In AO-1 and AO-2 most of the Core programme was devoted to the Galactic Center Deep Exposure (GCDE) and the Galactic plane Scans (GPS). The AO-1 IBIS survey programme (with a total exposure exceeding 5 Ms) has so far revealed the presence of ~120 sources detected down to ~1 mCrab. Most of them are identified with Galactic X-ray binary systems; 28 sources of the objects are of unknown nature. These sources account for most of the Milky Way's emission in hard X-rays/soft γ-rays, leaving at most a minor role for diffuse processes.

Although the INTEGRAL AO-1 and AO-2 Core program was not optimized for extragalactic studies, so far 11 AGN have been detected during the Galactic plane and Galactic Centre surveys; a few of them are new hard X-ray discoveries. Note that the main limitations in such a crowded field are the coded noise and background variation model. An example of a Galactic plane observation with two AGN detected in the field is given in Figure 16.

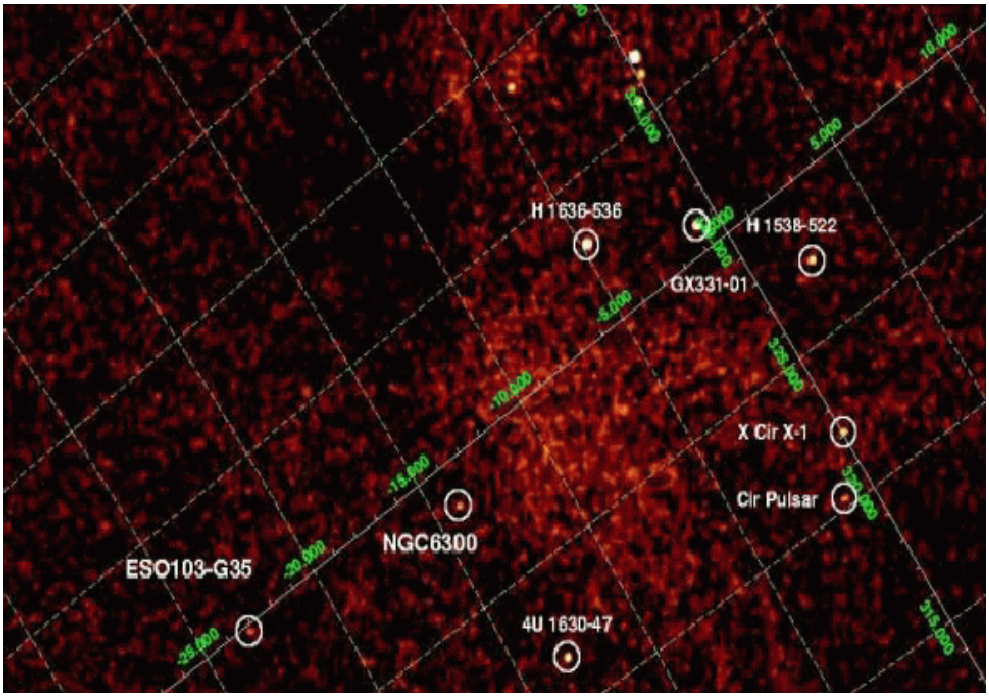

Figure 16. A typical 20-100 keV ISGRI mosaic image showing two Seyfert 2 systems (ESO103-G35 and NGC 6300) just above the Galactic plane.

2. IBIS sensitivity

Figures 17 and 18 show, respectively, the continuum (S_c) and line sensitivities (S_l), for ISGRI and PICsIT separately, as calculated from the prescriptions in Section V.3.3. The curves are for a detection of 3σ significance with an observing time of 10^5 s and 10^6 s, for the continuum and line sensitivities, respectively, taking into account in-flight background measurements. The continuum sensitivity is given for ΔE=E/2. The line sensitivity is for a narrow (unresolved) line. We also give (some of) the actual values in Tables 3, 4, and 5.

2.1 How to calculate observing times

The approximate signal-to-noise ratio for a given exposure can be calculated from the sensitivity curves. As shown in equations *V-3.3.1* and *V-3.3.2*,

the continuum sensitivity scales as

$\Delta E^{-1/2}$, $t^{-1/2}$ and n_σ,

the line sensitivity as $t^{-1/2}$ and n_σ.

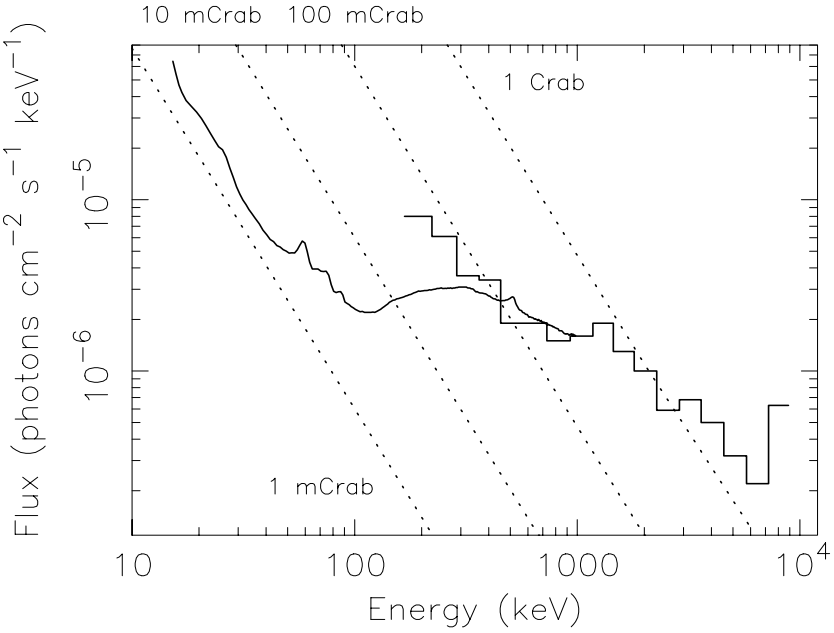

Figure 17. IBIS continuum sensitivities based on in-flight background measurements for a 10^5 s exposure, 3σ detection and continuum binned to ΔE= E/2. Systematic errors (such as background uniformity) are not taken into account. Solid line: ISGRI; solid stepped line: PICsIT (single and multiple events combined). Also shown (dotted lines) are the intensities of a 1, 10, 100 mCrab and 1 Crab source (photon spectral index Γ of -2).

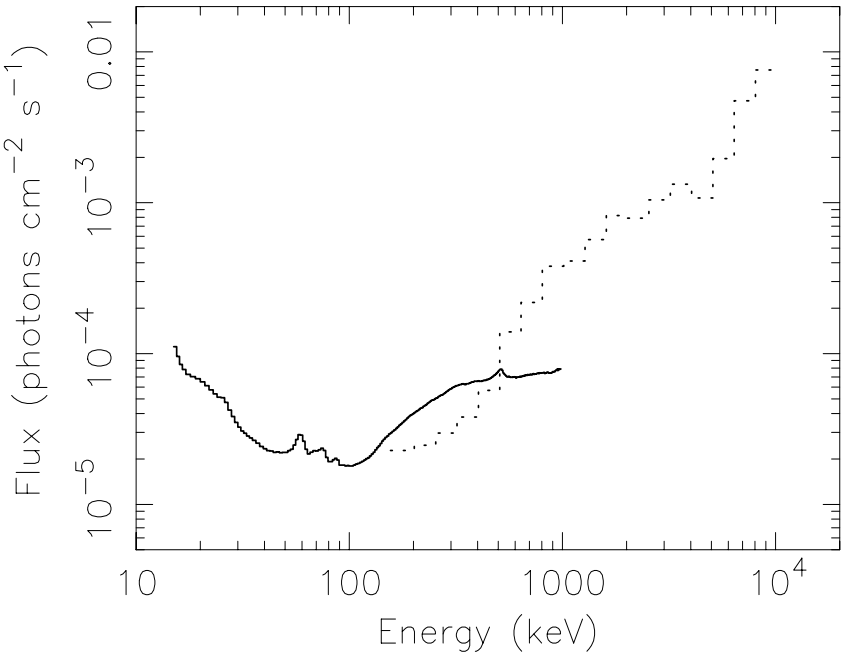

Figure 18. IBIS line sensitivities for a 10^6 s exposure, 3σ detection and an unresolved line. Solid line: ISGRI; dotted line: PICsIT.

Table 3: ISGRI continuum sensitivities (10^5 s exposure, 3σ detection, ΔE=E/2)

Energy (keV)	ph cm^{-2} s^{-1} keV^{-1}		Energy (keV)	ph cm^{-2} s^{-1} keV^{-1}		Energy (keV)	ph cm^{-2} s^{-1} keV^{-1}
15	69.3 x 10^{-6}		60	5.58 x 10^{-6}		300	3.09 x 10^{-6}
20	31.1 x 10^{-6}		70	3.83 x 10^{-6}		350	2.90 x 10^{-6}
25	20.0 x 10^{-6}		80	2.92 x 10^{-6}		400	2.74 x 10^{-6}
30	11.3 x 10^{-6}		90	2.53 x 10^{-6}		450	2.57 x 10^{-6}
35	8.06 x 10^{-6}		100	2.29 x 10^{-6}		500	2.66 x 10^{-6}
40	6.24 x 10^{-6}		150	2.60 x 10^{-6}		600	2.11 x 10^{-6}
45	5.40 x 10^{-6}		200	2.93 x 10^{-6}		700	1.93 x 10^{-6}
50	4.94 x 10^{-6}		250	3.03 x 10^{-6}		800	1.78 x 10^{-6}

Table 4: PICsIT continuum sensitivities (10^5 s exposure, 3σ detection, ΔE=E/2; single and multiple events combined)

Start energy (keV)	End energy (keV)	ph cm^{-2} s^{-1} keV^{-1}		Start energy (keV)	End energy (keV)	ph cm^{-2} s^{-1} keV^{-1}
170	220	7.99 x 10^{-6}		1200	1400	1.88 x 10^{-6}
220	280	6.06 x 10^{-6}		1400	1800	1.28 x 10^{-6}
280	370	3.62 x 10^{-6}		1800	2200	1.05 x 10^{-6}
370	430	3.41 x 10^{-6}		2200	2900	0.59 x 10^{-6}
430	580	1.90 x 10^{-6}		2900	3500	0.68 x 10^{-6}
580	720	1.91 x 10^{-6}		3500	4500	0.50 x 10^{-6}
720	900	1.48 x 10^{-6}		4500	5700	0.32 x 10^{-6}
900	1200	1.57 x 10^{-6}		5700	7100	0.22 x 10^{-6}

Table 5: IBIS line sensitivities (ISGRI and PICsIT, 10^6 s exposure, 3σ detection)

Energy (keV)	ISGRI line ph $cm^{-2}s^{-1}$	PICsIT line ph $cm^{-2}s^{-1}$		Energy (keV)	ISGRI line ph $cm^{-2}s^{-1}$	PICsIT line ph $cm^{-2}s^{-1}$
22.5	5.74×10^{-5}			566.1	6.97×10^{-5}	14×10^{-5}
28.4	3.83×10^{-5}			712.6	7.28×10^{-5}	22×10^{-5}
35.7	2.66×10^{-5}			897.2	7.54×10^{-5}	38×10^{-5}
45.0	2.21×10^{-5}			1129.5		$41x\ 10^{-5}$
56.6	2.69×10^{-5}			1421.9		57×10^{-5}
71.3	2.28×10^{-5}			1790.1		82×10^{-5}
89.7	1.89×10^{-5}			2253.6		79×10^{-5}
112.9	1.90×10^{-5}			2837.1		100×10^{-5}
142.2	2.58×10^{-5}			3571.7		$130x\ 10^{-5}$
179.0	3.50×10^{-5}	2.3×10^{-5}		4496.5		110×10^{-5}
225.4	4.50×10^{-5}	2.5×10^{-5}		5660.7		200×10^{-5}
283.7	5.53×10^{-5}	3.0×10^{-5}		7126.5		470×10^{-5}
357.2	6.31×10^{-5}	3.8×10^{-5}		8971.6		760×10^{-5}
449.6	6.74×10^{-5}	5.7×10^{-5}				

So the signal-to-noise ratio achieved for a different time, t(sec), ΔE/E and continuum or line flux N_c, N_l (photons $cm^{-2}\ s^{-1}\ keV^{-1}$ and photons $cm^{-2}\ s^{-1}$ respectively), would be:

$\mathbf{n_\sigma = 3(N_c/S_c)(2\Delta E/E)^{1/2}\ (t/10^5)^{1/2}}$ in the continuum and *VI-2.1*

$\mathbf{n_\sigma = 3(N_l/S_l)\ (t/10^6)^{1/2}}$ for a narrow (unresolved) line. *VI-2.2*

If the line is broad, with a FWHM of ΔE, then the signal-to-noise ratio is reduced by $(\Delta E/\delta E)^{1/2}$, where δE is the instrumental FWHM at that energy (see Figures 9 and 10).

Note: if the 5 x 5 dither pattern is used there is a 1.8% reduction in the achieved signal-to-noise ratio compared to the above. The hexagonal dither entails no loss.

2.2 Hints and warnings

The results arising from these calculations should be treated as approximations only and should be used only for a *preliminary* feasibility check for a potential observation. The *final* observation durations - those entered into the observing proposal - should be determined with the on-line observation time estimator (OTE), accessible via the Integral Science Operations Centre web site: **http://www.rssd.esa.int/integral/isoc/operations/html/OTE.html**.

The OTE will be used by ISOC to assess the technical feasibility of proposed observations, and advise the Time Allocation Committee (TAC) accordingly.

The continuum sensitivities (see Figures 17 and 18) are given for $\Delta E = E/2$ and can be extrapolated reliably to small energy ranges. However, when ΔE is greater than E/2, one in principle has to split the broad energy range into smaller energy bands, which all have individual ΔE smaller than E/2, then calculate the signal-to-noise or exposure times in each of these bands, and combine the results to get the appropriate values for the inital broad energy range. OTE now takes care of this (unlike in AO1 and AO-2), by doing the split itself assuming a power-law spectrum (where the observer is free to choose the value of the power-law index). The final OTE output is combined and presented into a single result. Note that other spectral models are not supported.

3. Worked-out examples

Here we give some examples of how equations *VI-2.1* and *VI-2.2*, as well as OTE, can be used to assess the feasibility of 'real' observations.

3.1 Example 1

For a hard transient with a flux of 100 mCrab at 100 keV and a hard power law (photon spectral index Γ of -1) continuum above 100 keV, determine the achievable signal-to-noise ratio at 100 keV in an energy bin corresponding to the instrument FWHM at that energy.

Extrapolating the 2-10 keV flux of the Crab to the gamma-ray band, using a photon spectral index Γ of -2.1, a 100 mCrab source has a flux at 100 keV of

$$\mathbf{N_c = 6.9 \times 10^{-5}\ photons\ cm^{-2}\ s^{-1}\ keV^{-1}}.$$

At 100 keV only ISGRI is sensitive (it is below the energy range of PICsIT). The sensitivity curve (Figure 17 or Table 3) gives a flux value at 100 keV of

$$\mathbf{S_c = 2.3 \times 10^{-6}\ photons\ cm^{-2}\ s^{-1}\ keV^{-1}}.$$

The energy resolution of ISGRI (FWHM, see Figure 9) at 100 keV is 8%;

$\Delta E/E = 0.08$.

Assume an observation time of 50 ksec;

$t = 5 \times 10^4$ **sec**.

This results in a signal-to-noise ratio (*VI-2.1*) of

$n_\sigma = 3 \times (6.9 \times 10^{-5} / 2.3 \times 10^{-6}) \times (2 \times 0.08)^{1/2} \times (5 \times 10^4 / 10^5)^{1/2} = 25\sigma$.

In comparison, the OTE indicates a 24σ detection for a 5x5 dither observation.
Note that OTE shows also that the source is easily detectable near 100 keV with ISGRI within 8.6 ksec for a signal-to-noise ratio of 10σ.

3.2 Example 2

Consider the same source as in Example 1, but at higher energies, i.e., 800 keV.

Extrapolation of the 100 keV flux with the hard power law described above gives a 800 keV flux of

$N_c = 8.5 \times 10^{-6}$ **photons** $cm^{-2}\ s^{-1}\ keV^{-1}$.

Both PICsIT and ISGRI are sensitive at 800 keV. The sensitivity curves (Figure 17 or Tables 3 and 4) indicate:

S_c **(ISGRI)** $= 1.8 \times 10^{-6}$ **photons** $cm^{-2}\ s^{-1}\ keV^{-1}$,
S_c **(PICsIT)** $= 1.5 \times 10^{-6}$ **photons** $cm^{-2}\ s^{-1}\ keV^{-1}$.

The overall sensitivity compared to source flux is lower at 800 keV compared to 100 keV, so use a larger energy bin, e.g.,

$\Delta E/E = 0.15$.

Again assume a 50 ksec observation;

$t = 5 \times 10^4$ **sec**.

Perform the same calculation as in Example 1;

n_σ **(ISGRI)** $= 5.5\sigma$,
n_σ **(PICsIT)** $= 6.6\sigma$.

In comparison, the OTE gives 5.3σ and 6.3σ, respectively, for a 5x5 dither observation.

ISGRI and PICsIT can be combined to increase the significance of the detection:

n_σ (total) = (n_σ (PICsIT)^2 + n_σ (ISGRI)^2)$^{1/2}$ = (5.3^2 + 6.3^2)$^{1/2}$ = 8.2σ.

OTE also shows that the source is detectable at 800 keV within 180 and 127 ksec, respectively with ISGRI and PICsIT, for a signal-to-noise ratio of 10σ.

3.3 Example 3

Consider the same transient as in the previous examples, but now the flux in only a broad band is known.

The source flux in, for example, the 50-150 keV band is

N_c = 7.6 x 10^{-5} photons cm^{-2} s^{-1} keV^{-1}.

Assume again a 50 ksec observation;

t = 5 x 10^4 sec.

Assuming a power-law spectrum (where we have input a photon spectral index of -1) OTE splits the 50-150 keV band into 3 smaller energy bands, i.e., 50-83 keV, 83-138 keV and 138-150 keV. In Table 6 we show the fluxes in these 3 bands as given by OTE, as well as the ISGRI sensitivities in these bands (see Figure 17 or Table 3), and calculate the significances using *VI-2.1 (*n_σ) and OTE (n_σ(OTE), assuming a 5x5 dither observation).

Table 6: OTE significance calculations for Example 3

Energy band (keV)	**Flux (ph cm^{-2} s^{-1} keV^{-1})**	**Sensitivity (ph cm^{-2} s^{-1} keV^{-1})**	**n_σ**	**n_σ(OTE; 5x5 dither)**
50-83	1.06 x 10^{-4}	5.0 x 10^{-6}	45	50
83-138	0.64 x 10^{-4}	2.4 x 10^{-6}	56	54
138-150	0.48 x 10^{-4}	2.6 x 10^{-6}	16	16

The calculated significances n_σ (4th column in Table 6) can be combined to determine the significance in the 50-150 keV band:

n_σ = 74σ**.**

OTE combines the significances to a single value for the 50-150 keV band: 75σ (assuming a 5x5 dither observation). Compare this with the value one would get by directly using *VI-2.1* for the 50-150 keV range: $n_\sigma = 3 \times (7.6 \times 10^{-4} / 2.3 \times 10^{-6}) \times (2 \times 100/100)^{1/2} \times (5 \times 10^5 / 10^6)^{1/2} = 99\sigma$, i.e., one would be somewhat too optimistic in the latter case.

To detect the source with signal-to-noise ratio of 10σ in the 50-150 keV band one would need an exposure time of about 800 sec, as determined with OTE.

3.4 Example 4

Observations of a recent transient to search for the ^{22}Na line at 1.275 MeV (half life of 3.5 yr).

Assume that the model-predicted line flux after outburst is

$\mathbf{N_l = 1 \times 10^{-3}}$ **photons cm^{-2} s^{-1}**.

The PICsIT line sensitivity curve (Figure 18 or Table 5) indicates

$\mathbf{S_l = 4.8 \times 10^{-4}}$ **photons cm^{-2} s^{-1}**.

Assume a 500 ksec observation;

$\mathbf{t = 5 \times 10^5}$ **sec**.

Then the line is detected at (*VI-2.2*):

$\mathbf{n_\sigma = 3 \times (1 \times 10^{-3} / 4.8 \times 10^{-4}) \times (5 \times 10^5 / 10^6)^{1/2} = 4.4\sigma}$**.**

In comparison, the OTE indicates a 4.1σ detection for a 5x5 dither observation.

With OTE one can determine that for a detection at the 10σ level one would have needed about 3 Msec.